Exchange Interaction of Strongly Anisotropic Tripodal Erbium Single-Ion Magnets with Metallic Surfaces

Jan Dreiser,[†,‡,*] Christian Wäckerlin,[§,#] Md. Ehesan Ali,[⊥] Cinthia Piamonteze,[‡] Fabio Donati,[†] Aparajita Singha,[†] Kasper Steen Pedersen,[∥] Stefano Rusponi,[†] Jesper Bendix,[∥] Peter M. Oppeneer,[⊥] Thomas A. Jung,[§] and Harald Brune[†]

[†]Institute of Condensed Matter Physics, Ecole Polytechnique Fédérale de Lausanne, CH-1015 Lausanne, Switzerland, [‡]Swiss Light Source, Paul Scherrer Institut, CH-5232 Villigen PSI, Switzerland, [§]Laboratory for Micro- and Nanotechnology, Paul Scherrer Institut, CH-5232 Villigen PSI, Switzerland, [⊥]Department of Physics and Astronomy, Uppsala University, Box 516, S-75120 Uppsala, Sweden, and [∥]Department of Chemistry, University of Copenhagen, DK-2100 Copenhagen, Denmark. [#]Present address: Institute of Condensed Matter Physics, Ecole Polytechnique Fédérale de Lausanne, CH-1015 Lausanne, Switzerland.

ABSTRACT We present a comprehensive study of Er(trensal) single-ion magnets deposited in ultrahigh vacuum onto metallic surfaces. X-ray photoelectron spectroscopy reveals that the molecular structure is preserved after sublimation, and that the molecules are physisorbed on Au(111) while they are chemisorbed on a Ni thin film on Cu(100) single-crystalline surfaces. X-ray magnetic circular dichroism (XMCD) measurements performed on Au(111) samples covered with molecular monolayers held at temperatures down to 4 K suggest that the easy axes of the strongly anisotropic molecules are randomly oriented. Furthermore XMCD indicates a weak antiferromagnetic exchange coupling between the single-ion magnets and the ferromagnetic Ni/Cu(100) substrate. For the latter case, spin-Hamiltonian fits to the XMCD $M(H)$ suggest a significant structural distortion of the molecules. Scanning tunneling microscopy reveals that the molecules are mobile on Au(111) at room temperature, whereas they are more strongly attached on Ni/Cu(100). X-ray photoelectron spectroscopy results provide evidence for the chemical bonding between Er(trensal) molecules and the Ni substrate. Density functional theory calculations support these findings and, in addition, reveal the most stable adsorption configuration on Ni/Cu(100) as well as the Ni—Er exchange path. Our study suggests that the magnetic moment of Er(trensal) can be stabilized *via* suppression of quantum tunneling of magnetization by exchange coupling to the Ni surface atoms. Moreover, it opens up pathways toward optical addressing of surface-deposited single-ion magnets.

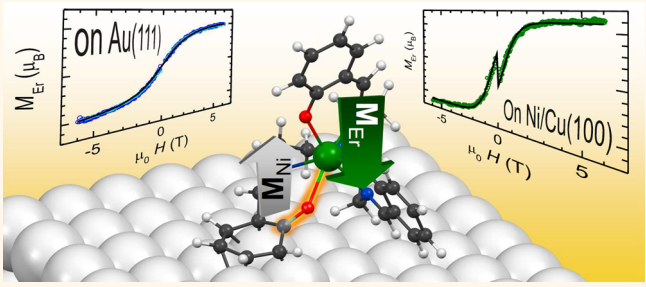

KEYWORDS: molecular magnets · single-ion magnets · sublimation · XMCD · XPS · STM · DFT

Molecular magnets[1] offer intriguing features such as slow relaxation of magnetization,[2,3] optical luminescence,[4,5] redox activity,[6,7] and spin crossover.[8] Therefore, such molecules are promising building blocks for multifunctional molecular spintronics applications.[9,10] To exploit molecular magnets they can be deposited in a monolayer or submonolayer coverage onto a suitable substrate.[11−13] This approach provides access to single molecules that could eventually be switched or read out by, *e.g.*, a scanning tunneling microscope (STM) tip[14−16] invigorating the dream of ultimate miniaturization. Currently there is emerging interest in surface-deposited molecular magnets that bring along properties or functionalities beyond the well-established paramagnetism of metal-phthalocyanines[17,18] and metal-porphyrins.[19−21]

Volatility is a desirable property since sublimation in ultrahigh vacuum largely avoids surface contamination. This is highly important for experiments that are sensitive to the molecule−surface interaction. By far not every molecular magnet, however, survives the sublimation since the molecule needs to be thermally stable at (or, even better, beyond) the sublimation temperature. Concerning the thermal stability, molecules containing a single magnetic ion and a single covalent backbone are especially promising since they are in general less fragile than polynuclear clusters. Nevertheless,

* Address correspondence to jan.dreiser@epfl.ch.

Received for review January 21, 2014 and accepted March 19, 2014.

Published online March 19, 2014
10.1021/nn500409u

several examples of sublimable polynuclear clusters have been demonstrated in the past.[22−24] So-called single-ion magnets[25−28] (SIMs) exhibit slow magnetization relaxation and are therefore an ideal realization of nanometer-sized quantum bits or magnetic storage elements containing only one spin-bearing system. In this context the rare-earth-based SIM $TbPc_2$ has been investigated on different surfaces.[29−31] Very recently, the magnetic properties of the lanthanide complex Er(trensal)[32] (H_3trensal = 2,2′,2″-tris(salicylideneimino)-triethylamine) have been studied in the bulk crystalline phase.[33,34] This new class of SIMs offers spectroscopic access to its ultrasharp 4f−4f optical transitions, which, *e.g.*, in $TbPc_2$ are largely masked by strong optical transitions on the ligand. These 4f−4f transitions may open up intriguing pathways for optical manipulation of the magnetization and provide independent handles to study the electronic structure of isolated molecules on surfaces. The structure of the pristine Er(trensal) molecule as obtained by X-ray diffraction is shown in Figure 1. The central Er^{III} ion is 7-fold coordinated to the trensal ligand giving rise to a 3-fold symmetry axis through the apical nitrogen atom where the three legs are connected. The rigidity of the ligand and the absence of counterions and solvent molecules provide the necessary stability for the molecule to withstand the sublimation process as well as the interaction with the metal surface. Furthermore, the molecule exhibits a strong magnetic anisotropy with the easy axis collinear with the molecular C_3 axis. Magnetization relaxation times of a few milliseconds in an applied magnetic field of ∼1 kOe are observed in SQUID measurements on powder samples and on a single crystal of Er(trensal) at low temperatures.[33,34] The Er(trensal) molecule represents a new class of trigonal, nonflat single-ion magnets. Moreover, the roundish-pyramidal shape of the Er(trensal) molecules results in a weaker preference for a specific adsorption geometry leading to richer adsorption properties, whereas flat molecules exhibit only a few adsorption conformations. This flexibility may open up future prospects, *e.g.*, in controlling or switching the orientation of the magnetic easy axis by molecule−surface interaction.

In this work we show, first, that Er(trensal) molecules can be sublimed and deposited onto metallic surfaces under ultrahigh vacuum conditions while they stay intact as a whole. Further, we characterize the adsorption properties and magnetic behavior of mono- and multilayers of Er(trensal) on Au(111) and on a ferromagnetic Ni thin film on Cu(100) by X-ray photoelectron spectroscopy (XPS), X-ray absorption spectroscopy (XAS), and X-ray magnetic circular dichroism (XMCD). Scanning tunneling microscopy (STM) yields information about the spatial arrangement of the molecules. Furthermore, density functional theory (DFT) calculations provide insight into the adsorption geometries of the molecule on Au and Ni surfaces and elucidate the dominant exchange path of the antiferromagnetic coupling between the SIM and the Ni surface.

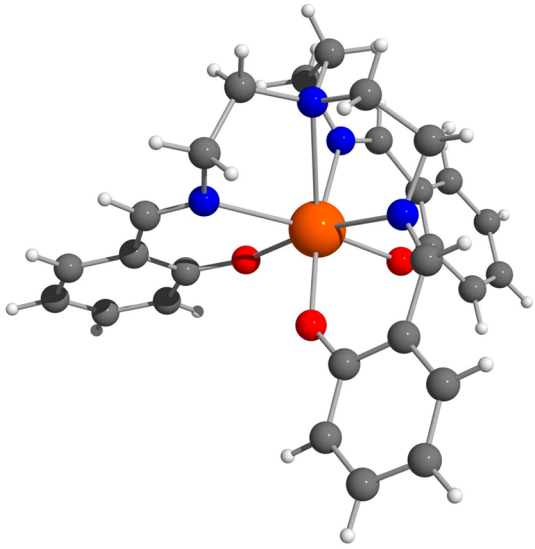

Figure 1. Molecular structure of the single-ion magnet Er(trensal). Color code: orange, Er; red, O; blue, N; gray, C; white, H.

RESULTS

Three different samples of Er(trensal) molecules deposited onto single crystalline metal substrates were investigated: (**A**) a thin film of ∼10 monolayers (MLs) of Er(trensal) on Au(111), (**B**) a ML on Au(111), and (**C**) a ML on a ferromagnetic Ni thin film[35] (∼15 monolayers of Ni) on Cu(100).

Sublimation and X-ray Photoelectron Spectroscopy. Deposition was performed at a crucible temperature of 557 K, which yielded a rate of ∼0.5 MLs per minute with a source-sample distance of 10 cm. During sublimation the chamber pressure was below 3×10^{-9} mbar indicating the sublimation of clean material in the absence of thermal decomposition. The XPS data obtained on samples **A**−**C** are plotted in Figure 2 clearly showing the presence of C, N, and O on the different surfaces. Er could only be observed in the XPS data of the multilayer (sample **A**) because of the weak 4d peak. The substrate Au 4f peaks are slightly larger in sample **B** compared to **A** (370 *vs* 312 kcounts peak intensity) consistent with the lower coverage. The peaks observed for C, N, and O are narrow, strongly suggesting that the Er(trensal) molecules are present in their pristine state on the surface. This is corroborated by the extracted stoichiometry presented in Table S1 (Supporting Information (SI)). The C 1s, N 1s and O 1s spectra measured on the multilayer and on the monolayer on Au(111) (samples **A** and **B**) are very similar concerning the peak energies (*cf.* Tables S2 and S3 (SI)) suggesting that the molecules are only weakly interacting with the Au(111) surface. On all samples, the split C 1s signal can be attributed to the different

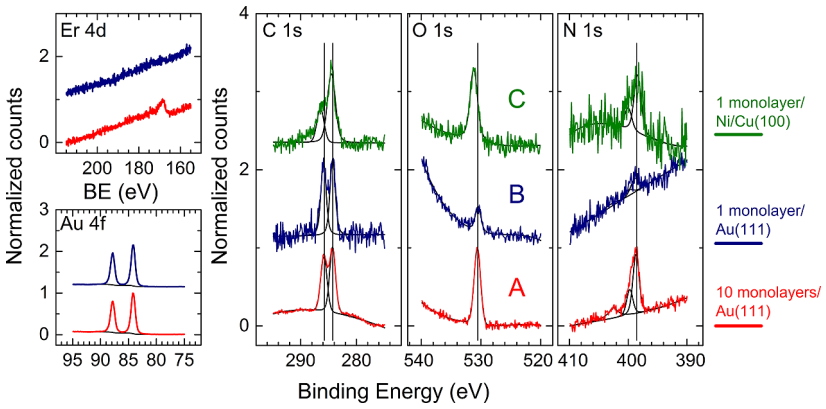

Figure 2. Core-level XPS spectra obtained on samples A (multilayer), B (1 monolayer on Au(111) and C (1 monolayer on Ni thin film on Cu(100)). Data and fits are plotted as colored and black solid lines, respectively. Thin vertical lines are guides to the eyes. The substrates were checked for cleanliness by XPS prior to the molecule deposition. Different scaling factors were applied to maximize visibility of the peaks. Peak areas are reported in the Supporting Information.

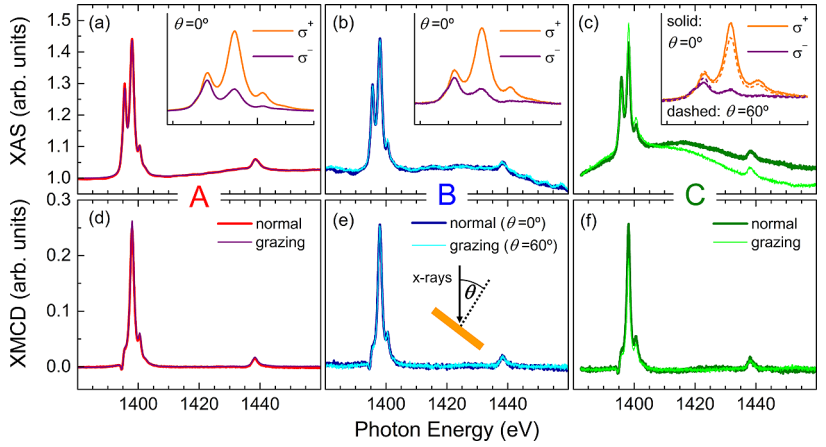

Figure 3. XAS and XMCD spectra recorded at the Er $M_{4,5}$ edges on samples A–C. Field and temperatures were $\mu_0 H = -6$ T (a–f) and $T = 11$ K (a,d), 6 K (b,e), and 4 K (c,f). The angle dependence indicates the absence (presence) of a preferred orientation of the molecules in samples A, B (sample C). The full polarization dependence for all samples is given in the Supporting Information.

chemical environments of the C atoms in the Er-(trensal) molecule. Here, the peak at higher energies (E = 285.85 eV in samples **A** and **B**) can be assigned to the C atoms that are bound to electron-withdrawing O or N, whereas the lower-energy peak (E = 284.3 eV in samples **A** and **B**) stems from the remaining C atoms.[36] Concerning the N 1s spectra, the observed signature on sample **A** is consistent with the presence of three nitrogen peaks. The two peaks at 398.7 and 399.8 eV can be attributed to the N atoms bonded to two or three C atoms, respectively, with the intensity ratio of 3:1 consistent with the molecular structure. The feature at 402.6 eV can be assigned to an electron emission combined with an excitation ("shake-up") of the ligand, which sets in at energies larger than 3 eV.[32] The O 1s spectrum can be fitted with a single peak (E = 530.6 and 530.5 eV in samples **A** and **B**, respectively). On the Ni surface (sample **C**) peak shifts with respect to the other samples are observed indicating chemisorption of the molecules, *i.e.*, the covalent-bond formation between substrate and molecules. Chemisorption on Ni is not unexpected on the basis of earlier studies on metal phthalocyanines and porphyrins[37−39] and is in line with the findings from DFT calculations, which will be presented below.

X-ray Absorption Spectroscopy and Magnetic Circular Dichroism. XAS and XMCD data of samples **A**–**C** measured at the Er $M_{4,5}$ edge are shown in Figure 3. The absorption spectra exhibit the characteristic triple-peak structure corresponding to the $\Delta J = 0, \pm 1$ transitions from the filled 3*d* to the open 4*f* shell of the Er^{III} ion[40] indicating that the Er ion retains its $^4I_{15/2}$ ground state also in close proximity to the metal surfaces. Ligand-field effects are virtually not seen in the $M_{4,5}$ XAS because of the dominating spin–orbit coupling and electron–electron interaction. The strong XMCD indicates a large Er magnetic moment in all samples. For samples **A** and **B** the XAS spectra for normal (θ = 0°) and grazing (θ = 60°) incidence superpose onto each other suggesting an isotropic response. In contrast, on sample **C** a linear dichroism emerges at the Er M_5 edge as evidenced by the different XAS measured for the two orientations

TABLE 1. Expectation Values of Spin (S_z) and Orbital (L_z) Angular Momentum Operators Extracted from Sum Rule Analyses of XMCD Data

		sample A multilayer on Au(111) [11 K]	sample B monolayer on Au(111) [6 K]	sample C monolayer on Ni/Cu(100) [4 K]
normal, $\theta = 0°$	$\langle L_z \rangle$	2.4(2)	2.5(3)	3.8(4)
	$\langle S_z \rangle$	0.8(1)	0.8(1)	1.2(1)
	$\langle L_z \rangle + 2\langle S_z \rangle$	**3.8(3)**	**4.1(4)**	**6.2(4)**
grazing, $\theta = 60°$	$\langle L_z \rangle$	2.5(2)	2.5(3)	3.0(3)
	$\langle S_z \rangle$	0.8(1)	0.8(1)	0.9(1)
	$\langle L_z \rangle + 2\langle S_z \rangle$	**4.1(3)**	**4.1(4)**	**4.9(3)**

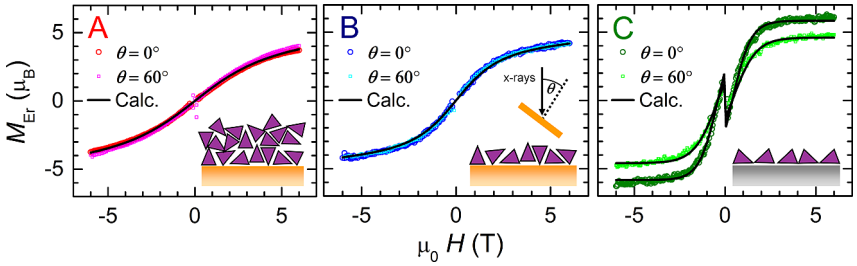

Figure 4. Field dependent magnetization of samples A–C. The temperatures were 11 K (sample A), 6 K (B), and 4 K (C). Symbols indicate data points, and solid lines represent calculations as described in the main text. The data reveals isotropic magnetization in samples A, B and weak antiferromagnetic coupling to the Ni substrate in sample C.

shown in Figure 3c and in the inset. Our measurements do not discriminate between X-ray natural linear dichroism (XNLD) and X-ray magnetic linear dichroism (XMLD), which result from the structure-induced and magnetic-field induced orientation of the Er 4f orbitals, respectively. Nevertheless, our observation of the linear dichroism, independent of whether it is XNLD or XMLD or both, indicates a preferred orientation of the molecules on the Ni surface. The XMCD reveals that the out-of-plane magnetization of the molecules is stronger than the in-plane magnetization at the same applied field of −6 T. A sum rule analysis[41,42] was performed in order to extract the absolute values of the spin and orbital magnetic moments. The number of holes was taken to be $n_h = 3$ consistent with the $4f^{11}$ configuration of Er^{III}, and $\langle T_z \rangle$ was calculated using the analytical formula given in ref 41. The results are summarized in Table 1 with the estimated experimental errors given in parentheses. For all samples, the $\langle L_z \rangle / \langle S_z \rangle$ ratio is lower than, but close to, the value of 6/1.5 = 4 expected from Hund's rules.

The Er magnetic moments found on samples **A** and **B** correspond to approximately half of the saturation magnetization of 9 μ_B expected for an isotropic paramagnet with $J = 15/2$ and the Er^{III} Landé g-factor $g_J = 6/5$. This finding, together with the absence of linear dichroism in samples **A** and **B**, can be rationalized by a random orientation of the molecules in these samples, while their magnetic anisotropy is still present. This interpretation is further supported by the magnetization curves displayed in Figure 4. They exhibit the typical S shape of a paramagnet. Sample **A** exhibits a slightly more shallow curve than sample **B**, which indicates a somewhat higher sample temperature during the experiment (*cf.* Experimental Section). Our spin-Hamiltonian simulations of an isotropically oriented powder of Er(trensal) using the magnetic anisotropy determined on bulk samples (see below) agree well with the experiment and confirm this picture. Sample **C** exhibits a remarkably different case. The X-ray spectra measured in large magnetic field (Figure 3) indicate a sizable Er magnetic moment, which is aligned parallel to the external field. However, in the vicinity of 0 T the Er magnetization is antiparallel, and it displays an abrupt jump according to the switching of the Ni thin film. Although the Ni film displays a small hysteresis opening,[35] it is not resolved in our measurements because of the scanning step size of $\Delta H = 1$ kOe. The field-dependent XMCD obtained at the Ni L_3 edge is given in the SI. The zero-field signature in the Er magnetization curve suggests the presence of a weak antiferromagnetic coupling between the molecules and the Ni film, which is broken already by a small applied field. The antiparallel orientation of Er and Ni magnetic moments without an applied magnetic field is also confirmed by XMCD spectra obtained in remanence (Figure 5) as well as by DFT-(GGA+U) calculations as described later in the text.

In order to obtain a quantitative understanding we have performed fits of different models to the experimental $M(H)$ curves. The Hamiltonian describing the ligand-field induced zero-field splitting of the Er-(trensal) molecules plus a Zeeman term reads

$$H = \sum_{k,-k \le q \le k} B_k^q \hat{O}_k^q(\mathbf{J}) + \mu_0 \mu_B g_J \hat{\mathbf{J}} \cdot \mathbf{H} \qquad (1)$$

This Hamiltonian operates on the $J = 15/2$ manifold of the $^4I_{15/2}$ ground-state multiplet of Er^{III}. All excited

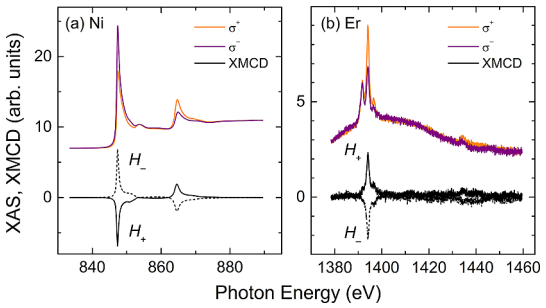

Figure 5. XAS and XMCD measured in remanence (T = 4 K) at normal incidence (a) at the Ni $L_{2,3}$ and (b) at the Er $M_{4,5}$ edges. For better visibility, the XAS is shown with an offset. The data directly visualizes the antiferromagnetic molecule−substrate coupling.

multiplets can be safely neglected because their contribution to the magnetism studied here is negligible.[33] The $\hat{O}_k^q$ are extended Stevens operators with coefficients B_k^q describing the zero-field splitting induced by the ligand field with parameters obtained from bulk samples in ref 33. As can be seen in Figure 4 the $M(H)$ curves of samples **A** and **B** can be fitted perfectly by assuming a powder sample with the same anisotropy as in the bulk. Note that in these calculations the sample temperature was adjusted to take into account different thermal conductivities arising from different mountings of samples **A** and **B** on *in situ* sample holders. It was impossible to fit the $M(H)$ curve of sample **C** with eq 1 even after including the Er−Ni exchange interaction by an empirical exchange field $\mathbf{H}_{ex}$ (see below). Also, taking into account in-plane or out-of-plane oriented molecules with anisotropy identical to the bulk did not lead to an acceptable reproduction of the experimental data. Therefore, we had to give up the primary assumption of the molecules preserving their bulk magnetic properties on Ni. In consequence we employed a more simplified description only considering the ground-state Kramers doublet of the Er^{III} ion given by

$$\begin{aligned} \hat{H} &= \mu_0\mu_B\hat{\tau}\cdot\mathbf{g}\cdot(\mathbf{H}+\mathbf{H}_{ex}) \\ \mathbf{H}_{ex} &= H_{0,ex}\cdot\mathrm{sgn}(\mathbf{H}\cdot\mathbf{e}_\theta)\cdot\mathbf{e}_\theta \end{aligned} \qquad (2)$$

where $\hat{\boldsymbol{\tau}}$ is the pseudospin-1/2 operator and $\mathbf{g}$ is the diagonal tensor with g_x, g_y, and g_z the perpendicular and longitudinal g-factors.[43] The coupling to the Ni substrate is taken into account *via* an exchange field $\mathbf{H}_{ex}$. Further, sgn is the sign function and $\mathbf{e}_\theta$ = (sin θ, 0, cos θ). For simplicity $\mathbf{H}_{ex}$ is assumed to be oriented always parallel to the external magnetic field, at an angle θ off the sample normal (the z direction). A fit to the data using eq 2 yields the best-fit parameters g_x = g_y = 8(1), g_z = 11.7(8) and $H_{0,ex}$ = −4(1) kOe; hence, the magnetic molecule−surface coupling is antiferromagnetic. Here, less anisotropy is observed than found in a previous SQUID study of single-crystalline Er(trensal) where the pseudospin-1/2 model gave g_x = g_y = 4.3, g_z =12.6.[33] From the average $g_{av} = (g_x + g_y + g_z)/3$ = 9.2 the exchange energy, *i.e.*, the energy difference between antiparallel and parallel orientations of the Er magnetic moment with respect to the Ni magnetization, can be determined to be $E_{ex} = g_{av}\mu_0\mu_B H_{0,ex}$ = 0.21 meV (1.7 cm^{-1}). DFT calculations presented below consistently reproduce the antiferromagnetic nature of the exchange coupling. The calculated magnitude of the exchange coupling constant is j_{DFT} = −87.88 cm^{-1}, giving rise to an exchange energy of $E_{ex,DFT}$ = 43.6 meV. Though this is quite a bit higher than the experimental observation, it is, however, not unexpected in view of existing shortcomings of DFT and the employed simplified Heisenberg spin-interaction picture between two localized spins on Er and on a Ni-atom on the surface. The exchange interaction was extracted from DFT calculations applying Noodleman's spin-projected broken-symmetry (BS) method.[44,45] The value for j_{DFT} quoted above is obtained by considering only the spin contribution S_{Er} = 3/2 of Er^{III}. If the total Er angular momentum of $J = L + S$ = 15/2 is used, the smaller value of j_{DFT} = −5.5 cm^{-1} is found.

The experimentally observed exchange energy of Er(trensal) is 1 order of magnitude smaller than the exchange energy found in $TbPc_2$ double deckers deposited on the same ferromagnetic out-of-plane Ni/Cu(100) substrate[31] and almost 2 orders of magnitude smaller than the exchange energy obtained for Fe-porphyrins on the same type of substrate (17 meV).[46] In a very recent study on $Gd_3N@C_{80}$ endofullerenes, also on Ni/Cu(100), the coexistence of antiferromagnetically and ferromagnetically coupled species was found with coupling strengths j in the order of a few meV[47] giving an estimated exchange energy of E_{ex} = 10−40 meV. These observations follow the trend that the magnetic exchange coupling between 3d and 4f magnetic moments is weaker than the 3d−3d coupling because of the localized nature of the 4f shell. This is also reflected in bulk measurements on polynuclear 3d−4f compounds.[48,49] The lower exchange energy in the present study compared to the studies of $TbPc_2$ and $Gd_3N@C_{80}$ mentioned before is perfectly consistent with the longer exchange coupling path in Er(trensal)/Ni/Cu(100) (see below).

Density Functional Theory Calculations. DFT+U calculations have been performed to obtain insight into the interactions between the Er(trensal) molecule and the Au(111) and Ni/Cu(100) surfaces. First, we performed molecular geometry optimizations placing the Er(trensal) molecules on three-layer slabs of Au and Ni, respectively. All geometry optimizations were performed by fully relaxing all degrees of freedom except for those of the atoms in the bottom substrate layer. We performed the calculations in three ways: First, the Er(trensal) molecules were placed on the surfaces with the C_3 axis normal and the tripod pointing down to the surface. Second, we performed Born−Oppenheimer

ab initio molecular dynamics (AIMD) simulations applying a simulated annealing algorithm to sample the space of reachable configurations and thereby to obtain globally optimized configurations. For this purpose, the sample was initially heated to 500 K, and gradually the temperature was decreased to 90 K. The AIMD simulations revealed a continuous movement of the Er(trensal) molecules on the surface. Several configurations from the AIMD trajectory were chosen, and the molecular geometry was again optimized for each of these. Third and last, we created two additional configurations that were not accessible in this AIMD trajectory called "tilted" and "top down" and optimized their positions. All optimized geometries are depicted and the corresponding adsorption energies are given in Figure S5 (SI). Our calculations reveal that the adsorption energies of all conformations differ by less than ~0.5 eV; *i.e.*, there is only very weak energetic preference for any of the specific configurations. Furthermore, there is no overlap of electron density between the Er(trensal) molecule and the Au substrate atoms. Hence, only noncovalent interactions, such as static dipolar interactions, play a role here. Altogether, our calculations show that the Er(trensal) molecules are physisorbed onto, or very weakly bound to, the Au(111) surface.

Conversely, on Ni our calculations reveal chemisorption, or a clear chemical interaction between the Er(trensal) and the surface Ni atoms. The most favorable configuration obtained from geometry optimization is shown in Figure 6. We found that the "tilted" configuration is the energetically most favorable configuration with an adsorption energy of $E_{tilted} = -6.22$ eV. In this configuration one of the benzene rings becomes quasiparallel to the substrate, which maximizes $p_\pi - d_\pi$ interactions between the Er(trensal) molecule and the Ni surface. This is also consistent with an increase of C−C bond lengths of the adsorbed benzene rings by 0.05 Å as compared to the other two bare benzene rings. Further, two other configurations (*cf.* Figure S6 (SI)) are found, with significantly weaker adsorption energies of $E_{top\text{-}up} = -4.51$ eV and $E_{top\text{-}down} = -1.28$ eV.

To understand the mechanism and pathway of the molecule−surface exchange interaction we have plotted the electron and spin density for the most stable, tilted, geometry (Figure 6). The 4f spin of Er^{III} is antiferromagnetically coupled to that of the Ni surface, as observed in the XMCD experiments. The projected spin magnetic moment located on the Er^{III} ion is computed to be $-2.72\ \mu_B$, which mainly arises from the three unpaired electrons in the localized 4f orbitals of Er. Because of Hund's rules and because of the very strong spin−orbit coupling ($\zeta \sim 2400\ cm^{-1}$) dominating over typical Zeeman energies the orbital magnetic moment is always parallel to that of the spin. A small amount of delocalized spin-down density, induced by the 4f spin, is found on the oxygen atoms. In the molecule−substrate interface region, the spin density is even smaller. The antiparallel spin of Er(trensal) on Ni/Cu(100) is hence driven by an indirect exchange coupling, which occurs through the chemical bonds. This is similar to the cases reported in refs 31, 37, 46, and 47, where exchange coupling is mediated by nonmagnetic O, N atoms or the carbon cage, respectively. Likewise, in the present study a large chemical species is involved in mediating the antiferromagnetic exchange, but in addition the exchange pathway is longer since it involves more than one nonmagnetic atom. The exchange interaction occurs through the ligand O atom bridging to the chemisorbed benzene ring. Further, it appears that the N atoms play a minor role in mediating the magnetic exchange. The spin-down density on the bridging O atom indicates that antiferromagnetic superexchange is the dominating exchange mechanism (*cf.* Figure 6b).

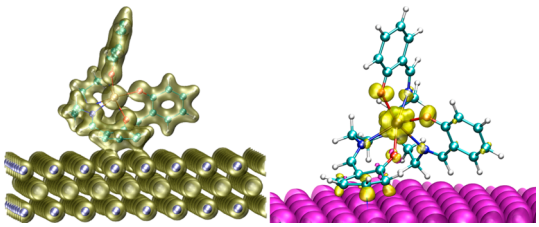

Figure 6. Calculated isosurfaces for the most-stable tilt geometry of electron density (left) and spin density (right) plotted at isovalues 0.001 a.u. Color code for (right): magenta and yellow correspond to spin-up and spin-down density, respectively. The occurrence of both spin-up and spin-down density on the oxygen atom bridging to the substrate-bonded benzene ring indicates antiferromagnetic superexchange interaction.

Scanning Tunneling Microscopy. STM images obtained at room temperature on Ni/Cu(100) and at 130 K on Au(111) are shown in Figure 7. The Er(trensal) molecules appear as roundish protrusions with a lateral size of ~1.2 nm fwhm, consistent with their structure determined by X-ray diffraction. In STM they appear without any visible internal structure. This is in contrast to a previous study where a functionalized Ga(trensal) complex with a more extended tripod structure was showing a "duck-foot" pattern.[50] On both Au and Ni substrates the molecules exhibit a uniform shape, except for some small details discussed below, confirming that the molecules are indeed intact on the surface. On the Ni surface the molecules are randomly distributed even at room temperature. Zoom-in images with drawn-in contour lines (Figure S8 (SI)) show that the molecules appear to be not perfectly round but slightly distorted. Since the distortion is observed in different directions in the same image, a scanning or tip induced artifact can be excluded. This suggests that the molecules indeed adsorb in the tilted geometry in agreement with the prediction by the DFT calculations described above. The small off-center distortion is consistent with the molecules being

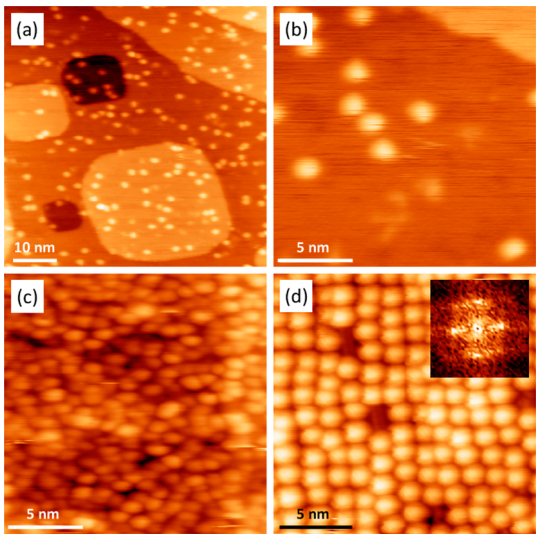

Figure 7. Constant-current STM images on a coverage of (a, b) 0.2 monolayer, (c) 1 monolayer of Er(trensal) on Ni/Cu(100), and (d) of 1 monolayer on Au(111). The inset in (d) is the 2D Fourier transform of the real-space image. The random distribution of the molecules on Ni and the quasiordering on Au indicate different absorption modes, *i.e.*, chemisorption on Ni *vs* physisorption on Au. Imaging parameters: (a) 1.05 V, 60 pA, (b) 1.05 V, 80 pA, (c) 2.1 V, 20 pA, (d) −1.5 V, −20 pA. (a−c) were taken at room temperature, (d) at T = 130 K.

rotated at random angles around the surface normal. The STM observations give strong support to the findings from XPS data and to the DFT calculations, which suggest that the molecules are chemisorbed. Also, this observation agrees well with the chemisorption observed for several metal-porphyrins on Co and Ni thin films.[37] On Au(111), imaging was only successful at 130 K. At room temperature, it was impossible to obtain stable imaging conditions because of frequent spikes in the tunnel current, which are most likely due to thermal motion or the movement of molecules by the STM tip. These observations are consistent with the physisorption of the molecules as found from the XPS and DFT evidence. However, it needs to be noted that the diffusion barrier is generally not indicative for the adsorption strength. The molecular arrangement exhibits some degree of local order between nearest neighbors (*cf.* inset of Figure 7d with the 2D Fourier transform). Since in the monolayer regime the formation of ordered patterns is determined by the subtle balance between molecule−substrate and molecule−molecule interactions as well as by the corrugation of the substrate surface,[21,37] the adsorption behavior of the Er(trensal) molecules observed here is not unexpected. Moreover, given the roundish shape of the molecules the observed quasiordering on Au can, but does not have to, be related to a preferential orientation.

DISCUSSION

The magnetic response of the molecules on Au can be reproduced by the bulk ligand-field parameters of Er(trensal); however, this is not possible for the Ni surface, even when assuming molecules adsorbed with a nonzero angle between the surface normal and their magnetic easy axes. This observation indicates a substrate-induced modification of magnetic properties on the Ni surface. Adsorption-induced structural changes of molecules have been previously observed in TCNQ/Cu systems.[51,52] Further, the adsorption-induced change of the magnetic anisotropy from easy-plane to easy-axis type has been observed in single Fe(II)-phthalocyanine molecules attached to an oxidized Cu(110) surface.[53] In this light, and given the results found in ref 33, where subtle structural modifications in Er(trensal) derivatives lead to dramatic changes in the magnetic properties, it is reasonable to assume that the observed magnetic behavior of sample **C** results from adsorption-induced structural distortions of the molecules on the Ni surface.

No hysteresis is observed in the XMCD measurements on all samples **A**−**C**. The absence of the Ni hysteresis in our data on sample **C** has already been discussed earlier in the text. Regarding the molecules themselves, no intrinsic hysteresis is expected either in view of the subsecond magnetization lifetimes, *i.e.*, ground-state lifetimes observed in the previous SQUID studies.[33,34] At low temperatures $T < 3$ K in the absence of a magnetic field the magnetization relaxation in Er(trensal) is dominated by quantum tunneling of magnetization (QTM).[33,34] QTM becomes very inefficient upon the application of a small magnetic field, which may also be the effective magnetic field resulting from exchange coupling, as it was previously demonstrated in a bulk measurement.[54] Hence our results suggest that the Er−Ni exchange coupling can act as a means to suppress QTM and thus to stabilize the magnetic moment of the Er(trensal) molecules on the ferromagnetic surface, albeit the ideal conditions for the suppression as extracted from bulk studies ($T <$ 3 K, $H \sim 1$ kOe) are almost, but not exactly met in this study. This is true while assuming that other, surface-related, mechanisms of magnetization relaxation are irrelevant.

The nonflat molecular structure leads to a significant spatial separation between the Er^{III} ion and the metal surface. This will result in a substantial decoupling of the localized 4f magnetic moment from the conduction-band electrons of the metal which, otherwise, could increase the magnetization relaxation rate over that of the bulk molecules by spin-flip scattering processes. Hence, the use of nonflat SIMs to realize single isolated magnetic computing or storage elements represents a promising alternative to decoupling-layer[55] or symmetry-based[56] approaches.

CONCLUSIONS

We have studied monolayers of the single-ion magnet Er(trensal) deposited on Au(111) and on a Ni thin

film on Cu(100) by XPS, XAS, XMCD, and STM experiments as well as by DFT+U calculations. On Au(111), the molecules are weakly bound and exhibit random orientations of their magnetic easy axes and no significant changes of the magnetic behavior compared to bulk powder samples are detected. In contrast, XPS data for the molecules on Ni/Cu(100) suggest covalent bond formation between the molecules and the Ni surface. This observation is further supported by STM observations and DFT calculations. XMCD reveals that at zero magnetic field the Er magnetic moment is antiparallel to that of the Ni film; *i.e.*, the molecules are antiferromagnetically coupled to the substrate. Consistently, DFT+U calculations suggest that antiferromagnetic superexchange is the dominant coupling mechanism. The experimentally obtained exchange energy of $E_{ex} = 0.21$ meV is at least 1 order of magnitude smaller than reported in other studies of magnetically coupled molecule−substrate systems, consistent with the longer magnetic exchange path *via* the benzene ring and the oxygen atom. The anisotropic magnetic response of the molecules at large field indicates that they have a preferential orientation on Ni. The magnetic response cannot be modeled using the bulk anisotropy parameters of the molecules together with an empirical exchange field, which points to an adsorption-induced structural distortion of the molecules. DFT calculations suggest that in the most stable configuration one of the benzene rings is parallel to the Ni surface consistent with a slightly asymmetric shape of the molecules in the STM observations. Our results suggest that the magnetic moment of the Er(trensal) molecules can be stabilized *via* suppression of quantum tunneling of magnetization due to the weak Er−Ni magnetic exchange coupling. Furthermore, this study paves the way for the optical investigation, addressing and control of large single magnetic moments on surfaces realized in Er(trensal) SIMs.

METHODS

Synthesis of Er(trensal). The bulk sample was prepared by a modification of the procedure described by Kanesato and Yokoyama[57] as outlined in ref 33. All starting materials were purchased from commercial sources and employed without further purification. The phase purity of the employed samples was checked by X-ray powder diffraction and elemental analysis.

Substrate Preparation and Molecule Sublimation. The Au(111) and Cu(100) single crystalline substrates were prepared by several cycles of Ar^+ sputtering and annealing in a UHV system with a base pressure of 2×10^{-10} mbar, equipped with XPS and STM. Er(trensal) was deposited from a Knudsen cell, and the sublimation rate was measured using a quartz crystal balance. The characterization of the Ni/Cu(100) film by STM, XPS and XAS/XMCD is reported in the Supporting Information.

X-ray Absorption Spectroscopy. The X-ray absorption measurements were carried out at the X-Treme beamline[58] of the Swiss Light Source. Prior to the XAS measurements, the coverage with molecules was checked by XPS. Samples were then transported from the XPS/STM system to the XAS chamber without breaking the vacuum by use of a vacuum suitcase. Absorption spectra were acquired in on-the-fly mode.[59] The full set of angle- and polarization-dependent spectra normalized to the pre-edge absorption is given in the Supporting Information. Field-dependent magnetization $M(H)$ was obtained by taking the difference of the absorption on the M_5 edge and the preedge. The curves were then scaled according to the total magnetic moment found from sum rules. The two Au(111) crystals used for samples **A** and **B** were mounted in a stainless steel cup (**A**) or directly (**B**) on stainless steel plates, while sample **C** was mounted on a tantalum plate. For this reason the lowest temperature of 4 K could only be reached for sample **C**. The temperatures of samples **A** and **B** were obtained as the only free parameter from model eq 1.

X-ray Photoelectron Spectroscopy. XPS measurements were carried out in the XPS/STM chamber mentioned before. The energy of the incident X-rays used in the XPS measurements was 1487.61 eV (Al Kα with monochromator). The instrumental setup in combination with the used lens mode and pass energy (20 eV) gives a resolution of 0.8 eV (full width at half-maximum). The energy calibration was performed using an Ar^+ sputtered Au reference, setting 84.0 eV at the Au $4f_{7/2}$ peak.

Scanning Tunneling Microscopy. Images were taken in the XPS/STM chamber in constant-current mode at room temperature and at 130 K with a commercial (SPECS Aarhus 150) STM. Electrochemically etched and *in situ* sputtered W tips were used.

Spin-Hamiltonian Calculations. Calculations were performed using a home-written MATLAB code. The magnetization was obtained by full diagonalization of the Hamiltonians given in the text and application of thermal statistics. Directional averaging was performed by employing a Lebedev−Laikov grid.[60] The matrix representations of the extended Stevens operators were generated using the *stev* function from the EasySpin software package.[61]

Density Functional Theory Calculations. To perform the DFT calculations on the metallic film we have constructed a simulation cell consisting of three atomic layers using 8×8 repetitions of the Au or Ni unit cells. Hence each layer contains 64 Au/Ni atoms. The lattice parameters were obtained from experimentally reported values of 4.08 Å for Au. The issue of optimizing the lattice parameters for Au was discussed previously; it was noted that, depending on the computational functional, the optimized lattice constant of Au varies from 4.06 (LDA), 4.15 (PW91) to 4.24 Å (BLYP).[62−64] However, as differences between bulk lattice parameters and those of reconstructed surfaces are expected, we opted here for the experimental value. Similarly for Ni the considered lattice parameter is 3.52 Å. Previous DFT investigations[38,39] of molecule−surface interactions have shown that the metallic surface is well described by three atomic layers, in particular with a sufficiently large k-mesh.[65] The DFT calculations have been performed applying the generalized gradient approximation (GGA) for the initial geometry optimizations and the GGA+U approach for magnetic states calculations. In the latter case the on-site Coulomb correlations are taken into account only for the Er electrons. The U and J_{on} on-site values were chosen as 6.0 and 1.0 eV, respectively, on the 5d states of Er to prevent their spurious fractional occupations. This occurs due to the self-interaction error present in DFT functionals. The applied U and J_{on} on-site values are in the commonly accepted range for 4f elements.[66] The full-potential plane-wave code VASP has been used for the calculations in the present work, applying pseudopotentials within the projector augmented wave method.[67−69] The applied kinetic energy cutoff for the plane wave is 400 eV, and the chosen parametrization of the GGA exchange-correlation functional is PBE.[70] For the reciprocal space sampling $1 \times 1 \times 1$ as well as $2 \times 2 \times 2$ Monkhorst-Pack k-point mesh were used.

Conflict of Interest: The authors declare no competing financial interest.

Acknowledgment. We thank Rolf Schelldorfer and Marcus Schmidt for technical aid. J.D. and C.W. acknowledge funding by

an Ambizione grant (No. PZ00P2_142474) of the Swiss National Science Foundation. A.S. gratefully acknowledges funding from the Swiss National Science Foundation. Md.E.A. and P.M.O. acknowledge funding received from the Swedish Research Council (VR) as well as support from the Swedish National Infrastructure for Computing (SNIC). J.B. acknowledges support from the Danish Research Council for Independent Research (12-125226). T.J. gratefully acknowledges financial support from the Swiss Nanoscience Institute (SNI), Swiss National Science Foundation (Grants No. 200020-137917, 206021- 113149, 206021-121461).

Supporting Information Available: Stoichiometry from XPS, polarization-dependent XAS and XMCD spectra on samples **A**–**C**, DFT-optimized geometries of Er(trensal) on Au(111) and on Ni/Cu(100), zoom of STM images of Er(trensal) on Ni/Cu(100), XAS and STM characterization of the Ni/Cu(100) thin film. This material is available free of charge *via* the Internet at http://pubs.acs.org.

REFERENCES AND NOTES

1. Gatteschi, D.; Sessoli, R.; Villain, J. *Molecular Nanomagnets*; Oxford University Press: Oxford, U.K., 2006.
2. Caneschi, A.; Gatteschi, D.; Sessoli, R.; Barra, A. L.; Brunel, L. C.; Guillot, M. Alternating Current Susceptibility, High Field Magnetization, and Millimeter Band EPR Evidence for a Ground $S = 10$ State in $[Mn_{12}O_{12}(CH_3COOCH_3COO)_{16}(H_2O)_4]\cdot 2CH_3COOH\cdot 4H_2O$. *J. Am. Chem. Soc.* **1991**, *113*, 5873–5874.
3. Sessoli, R.; Gatteschi, D.; Caneschi, A.; Novak, M. A. Magnetic Bistability in a Metal-Ion Cluster. *Nature* **1993**, *365*, 141–143.
4. Beedle, C. C.; Stephenson, C. J.; Heroux, K. J.; Wernsdorfer, W.; Hendrickson, D. N. Photoluminescent Mn_4 Single-Molecule Magnet. *Inorg. Chem.* **2008**, *47*, 10798–10800.
5. Cucinotta, G.; Perfetti, M.; Luzon, J.; Etienne, M.; Car, P.-E.; Caneschi, A.; Calvez, G.; Bernot, K.; Sessoli, R. Magnetic Anisotropy in a Dysprosium/DOTA Single-Molecule Magnet: Beyond Simple Magneto-Structural Correlations. *Angew. Chem., Int. Ed.* **2012**, *51*, 1606–1610.
6. Freedman, D. E.; Jenkins, D. M.; Iavarone, A. T.; Long, J. R. A Redox-Switchable Single-Molecule Magnet Incorporating $[Re(CN)_7]^{3-}$. *J. Am. Chem. Soc.* **2008**, *130*, 2884–2885.
7. Gonidec, M.; Davies, E. S.; McMaster, J.; Amabilino, D. B.; Veciana, J. Probing the Magnetic Properties of Three Interconvertible Redox States of a Single-Molecule Magnet with Magnetic Circular Dichroism Spectroscopy. *J. Am. Chem. Soc.* **2010**, *132*, 1756–1757.
8. Gütlich, P.; Goodwin, H. A. *Spin Crossover in Transition Metal Compounds*; Springer: Berlin, 2004.
9. Rocha, A. R.; Garcia-suarez, V. M.; Bailey, S. W.; Lambert, C. J.; Ferrer, J.; Sanvito, S. Towards Molecular Spintronics. *Nat. Mater.* **2005**, *4*, 335–339.
10. Bogani, L.; Wernsdorfer, W. Molecular Spintronics Using Single-Molecule Magnets. *Nat. Mater.* **2008**, *7*, 179–186.
11. Mannini, M.; Pineider, F.; Sainctavit, P.; Danieli, C.; Otero, E.; Sciancalepore, C.; Talarico, A. M.; Arrio, M.-A.; Cornia, A.; Gatteschi, D.; *et al.* Magnetic Memory of a Single-Molecule Quantum Magnet Wired to a Gold Surface. *Nat. Mater.* **2009**, *8*, 194–197.
12. Domingo, N.; Bellido, E.; Ruiz-Molina, D. Advances on Structuring, Integration and Magnetic Characterization of Molecular Nanomagnets on Surfaces and Devices. *Chem. Soc. Rev.* **2011**, *41*, 258–302.
13. Mas-Torrent, M.; Crivillers, N.; Mugnaini, V.; Ratera, I.; Rovira, C.; Veciana, J. Organic Radicals on Surfaces: Towards Molecular Spintronics. *J. Mater. Chem.* **2009**, *19*, 1691–1695.
14. Schmaus, S.; Bagrets, A.; Nahas, Y.; Yamada, T. K.; Bork, A.; Bowen, M.; Beaurepaire, E.; Evers, F.; Wulfhekel, W. Giant Magnetoresistance through a Single Molecule. *Nat. Nano.* **2011**, *6*, 185–189.
15. Komeda, T.; Isshiki, H.; Liu, J.; Zhang, Y.-F.; Lorente, N.; Katoh, K.; Breedlove, B. K.; Yamashita, M. Observation and Electric Current Control of a Local Spin in a Single-Molecule Magnet. *Nat. Commun.* **2011**, *2*, 217.
16. Schwöbel, J.; Fu, Y.; Brede, J.; Dilullo, A.; Hoffmann, G.; Klyatskaya, S.; Ruben, M.; Wiesendanger, R. Real-Space Observation of Spin-Split Molecular Orbitals of Adsorbed Single-Molecule Magnets. *Nat. Commun.* **2012**, *3*, 953.
17. Wang, Y.; Wu, K.; Kroger, J.; Berndt, R. Review Article: Structures of Phthalocyanine Molecules on Surfaces Studied by STM. *AIP Adv.* **2012**, *2*, 041402.
18. Yoshimoto, S.; Kobayashi, N. Supramolecular Nanostructures of Phthalocyanines and Porphyrins at Surfaces Based on the "Bottom-Up Assembly". In *Functional Phthalocyanine Molecular Materials*; Jiang, J., Ed.; Springer: Berlin, 2010; Structure and Bonding, pp 137–167.
19. Jung, T. A.; Schlittler, R. R.; Gimzewski, J. K. Conformational Identification of Individual Adsorbed Molecules with the STM. *Nature* **1997**, *386*, 696–698.
20. Otsuki, J. STM Studies on Porphyrins. *Coord. Chem. Rev.* **2010**, *254*, 2311–2341.
21. Barth, J. V. Molecular Architectonic on Metal Surfaces. *Annu. Rev. Phys. Chem.* **2007**, *58*, 375–407.
22. Ghirri, A.; Corradini, V.; Bellini, V.; Biagi, R.; del Pennino, U.; De Renzi, V.; Cezar, J. C.; Muryn, C. A.; Timco, G. A.; Winpenny, R. E. P.; *et al.* Self-Assembled Monolayer of Cr_7Ni Molecular Nanomagnets by Sublimation. *ACS Nano* **2011**, *5*, 7090–7099.
23. Margheriti, L.; Mannini, M.; Sorace, L.; Gorini, L.; Gatteschi, D.; Caneschi, A.; Chiappe, D.; Moroni, R.; de Mongeot, F. B.; Cornia, A.; *et al.* Thermal Deposition of Intact Tetrairon(III) Single-Molecule Magnets in High-Vacuum Conditions. *Small* **2009**, *5*, 1460–1466.
24. Rancan, M.; Sedona, F.; Marino, M. D.; Armelao, L.; Sambi, M. Chromium Wheels Quasi-Hexagonal 2D Assembling by Direct UHV Sublimation. *Chem. Commun.* **2011**, *47*, 5744–5746.
25. Ishikawa, N.; Sugita, M.; Ishikawa, T.; Koshihara, S.-y.; Kaizu, Y. Lanthanide Double-Decker Complexes Functioning as Magnets at the Single-Molecular Level. *J. Am. Chem. Soc.* **2003**, *125*, 8694–8695.
26. AlDamen, M. A.; Clemente-Juan, J. M.; Coronado, E.; Martí-Gastaldo, C.; Gaita-Ariño, A. Mononuclear Lanthanide Single-Molecule Magnets Based on Polyoxometalates. *J. Am. Chem. Soc.* **2008**, *130*, 8874–8875.
27. Jiang, S.-D.; Wang, B.-W.; Sun, H.-L.; Wang, Z.-M.; Gao, S. An Organometallic Single-Ion Magnet. *J. Am. Chem. Soc.* **2011**, *133*, 4730–4733.
28. Westerström, R.; Dreiser, J.; Piamonteze, C.; Muntwiler, M.; Weyeneth, S.; Brune, H.; Rusponi, S.; Nolting, F.; Popov, A.; Yang, S.; *et al.* An Endohedral Single-Molecule Magnet with Long Relaxation Times: $DySc_2N@C_{80}$. *J. Am. Chem. Soc.* **2012**, *134*, 9840–9843.
29. Katoh, K.; Yoshida, Y.; Yamashita, M.; Miyasaka, H.; Breedlove, B. K.; Kajiwara, T.; Takaishi, S.; Ishikawa, N.; Isshiki, H.; Zhang, Y. F.; *et al.* Direct Observation of Lanthanide(III)-Phthalocyanine Molecules on Au(111) by Using Scanning Tunneling Microscopy and Scanning Tunneling Spectroscopy and Thin-Film Field-Effect Transistor Properties of Tb(III)- and Dy(III)-Phthalocyanine Molecules. *J. Am. Chem. Soc.* **2009**, *131*, 9967–9976.
30. Stepanow, S.; Honolka, J.; Gambardella, P.; Vitali, L.; Abdurakhmanova, N.; Tseng, T.-C.; Rauschenbach, S.; Tait, S. L.; Sessi, V.; Klyatskaya, S.; *et al.* Spin and Orbital Magnetic Moment Anisotropies of Monodispersed Bis(Phthalocyaninato)-Terbium on a Copper Surface. *J. Am. Chem. Soc.* **2010**, *132*, 11900–11901.
31. Lodi Rizzini, A.; Krull, C.; Balashov, T.; Kavich, J. J.; Mugarza, A.; Miedema, P. S.; Thakur, P. K.; Sessi, V.; Klyatskaya, S.; Ruben, M.; *et al.* Coupling Single Molecule Magnets to Ferromagnetic Substrates. *Phys. Rev. Lett.* **2011**, *107*, 177205.
32. Flanagan, B. M.; Bernhardt, P. V.; Krausz, E. R.; Lüthi, S. R.; Riley, M. J. Ligand-Field Analysis of an Er(III) Complex with a Heptadentate Tripodal N_4O_3 Ligand. *Inorg. Chem.* **2001**, *40*, 5401–5407.
33. Pedersen, K. S.; Ungur, L.; Sigrist, M.; Sundt, A.; Schau-Magnussen, M.; Vieru, V.; Mutka, H.; Rols, S.; Weihe, H.; Waldmann, O.; *et al.* Modifying the Properties of 4f Single-Ion Magnets by Peripheral Ligand Functionalisation. *Chem. Sci.* **2014**, *5*, 1650–1660.

34. Lucaccini, E.; Sorace, L.; Perfetti, M.; Costes, J.-P.; Sessoli, R. Beyond the Anisotropy Barrier: Slow Relaxation of the Magnetization in Both Easy-Axis and Easy-Plane Ln(trensal) Complexes. *Chem. Commun.* **2014**, *50*, 1648–1651.
35. Huang, F.; Kief, M. T.; Mankey, G. J.; Willis, R. F. Magnetism in the Few-Monolayers Limit: A Surface Magneto-Optic Kerr-Effect Study of the Magnetic Behavior of Ultrathin Films of Co, Ni, and Co-Ni Alloys on Cu(100) and Cu(111). *Phys. Rev. B: Condens. Matter Mater. Phys.* **1994**, *49*, 3962–3971.
36. Moulder, J. F.; Stickle, W. F.; Sobol, P. E.; Bomben, K. D. *Handbook of X-ray Photoelectron Spectroscopy*; Chastain, J., King, R. C., Eds.; Physical Electronics, Inc.: Eden Prairie, MN, 1995; p 41.
37. Chylarecka, D.; Wäckerlin, C.; Kim, T. K.; Müller, K.; Nolting, F.; Kleibert, A.; Ballav, N.; Jung, T. A. Self-Assembly and Superexchange Coupling of Magnetic Molecules on Oxygen-Reconstructed Ferromagnetic Thin Film. *J. Phys. Chem. Lett.* **2010**, *1*, 1408–1413.
38. Wäckerlin, C.; Tarafder, K.; Siewert, D.; Girovsky, J.; Hählen, T.; Iacovita, C.; Kleibert, A.; Nolting, F.; Jung, T. A.; Oppeneer, P. M.; *et al.* On-Surface Coordination Chemistry of Planar Molecular Spin Systems: Novel Magnetochemical Effects Induced by Axial Ligands. *Chem. Sci.* **2012**, *3*, 3154–3160.
39. Wäckerlin, C.; Maldonado, P.; Arnold, L.; Shchyrba, A.; Girovsky, J.; Nowakowski, J.; Ali, Md. E.; Hählen, T.; Baljozovic, M.; Siewert, D.; *et al.* Magnetic Exchange Coupling of a Synthetic Co(II)-Complex to a Ferromagnetic Ni Substrate. *Chem. Commun.* **2013**, *49*, 10736–10738.
40. Thole, B. T.; Laan, G.; van der Fuggle, J. C.; Sawatzky, G. A.; Karnatak, R. C.; Esteva, J.-M. 3d X-ray-Absorption Lines and the $3d^9 4f^{n+1}$ Multiplets of the Lanthanides. *Phys. Rev. B: Condens. Matter Mater. Phys.* **1985**, *32*, 5107–5118.
41. Carra, P.; Thole, B. T.; Altarelli, M.; Wang, X. X-ray Circular Dichroism and Local Magnetic Fields. *Phys. Rev. Lett.* **1993**, *70*, 694–697.
42. Thole, B. T.; Carra, P.; Sette, F.; van der Laan, G. X-ray Circular Dichroism as a Probe of Orbital Magnetization. *Phys. Rev. Lett.* **1992**, *68*, 1943–1946.
43. Abragam, A.; Bleaney, B. *Electron Paramagnetic Resonance of Transition Ions*, Clarendon Press: Gloucestershire, U.K., 1970.
44. Noodleman, L. Valence Bond Description of Antiferromagnetic Coupling in Transition Metal Dimers. *J. Chem. Phys.* **1981**, *74*, 5737–5743.
45. Ali, Md. E.; Datta, S. N. Broken-Symmetry Density Functional Theory Investigation on Bis-Nitronyl Nitroxide Diradicals: Influence of Length and Aromaticity of Couplers. *J. Phys. Chem. A* **2006**, *110*, 2776–2784.
46. Bernien, M.; Miguel, J.; Weis, C.; Ali, Md. E.; Kurde, J.; Krumme, B.; Panchmatia, P. M.; Sanyal, B.; Piantek, M.; Srivastava, P.; *et al.* Tailoring the Nature of Magnetic Coupling of Fe-Porphyrin Molecules to Ferromagnetic Substrates. *Phys. Rev. Lett.* **2009**, *102*, 047202.
47. Hermanns, C. F.; Bernien, M.; Krüger, A.; Schmidt, C.; Waßerroth, S. T.; Ahmadi, G.; Heinrich, B. W.; Schneider, M.; Brouwer, P. W.; Franke, K. J.; *et al.* Magnetic Coupling of $Gd_3N@C_{80}$ Endohedral Fullerenes to a Substrate. *Phys. Rev. Lett.* **2013**, *111*, 167203.
48. Sessoli, R.; Powell, A. K. Strategies towards Single Molecule Magnets Based on Lanthanide Ions. *Coord. Chem. Rev.* **2009**, *253*, 2328–2341.
49. Dreiser, J.; Pedersen, K. S.; Piamonteze, C.; Rusponi, S.; Salman, Z.; Ali, Md. E.; Schau-Magnussen, M.; Thuesen, C. A.; Piligkos, S.; Weihe, H.; *et al.* Direct Observation of a Ferri-to-Ferromagnetic Transition in a Fluoride-Bridged 3d−4f Molecular Cluster. *Chem. Sci.* **2012**, *3*, 1024–1032.
50. Schramm, A.; Stroh, C.; Dössel, K.; Lukas, M.; Fischer, M.; Schramm, F.; Fuhr, O.; Löhneysen, H. v.; Mayor, M. Tripodal M(III) Complexes on Au(111) Surfaces: Towards Molecular "Lunar Modules". *Eur. J. Inorg. Chem.* **2013**, *2013*, 70–79.
51. Romaner, L.; Heimel, G.; Brédas, J.-L.; Gerlach, A.; Schreiber, F.; Johnson, R. L.; Zegenhagen, J.; Duhm, S.; Koch, N.; Zojer, E. Impact of Bidirectional Charge Transfer and Molecular Distortions on the Electronic Structure of a Metal-Organic Interface. *Phys. Rev. Lett.* **2007**, *99*, 256801.
52. Tseng, T.-C.; Urban, C.; Wang, Y.; Otero, R.; Tait, S. L.; Alcamí, M.; Écija, D.; Trelka, M.; Gallego, J. M.; Lin, N.; *et al.* Charge-Transfer-Induced Structural Rearrangements at Both Sides of Organic/Metal Interfaces. *Nat. Chem.* **2010**, *2*, 374–379.
53. Tsukahara, N.; Noto, K.; Ohara, M.; Shiraki, S.; Takagi, N.; Takata, Y.; Miyawaki, J.; Taguchi, M.; Chainani, A.; Shin, S.; *et al.* Adsorption-Induced Switching of Magnetic Anisotropy in a Single Iron(II) Phthalocyanine Molecule on an Oxidized Cu(110) Surface. *Phys. Rev. Lett.* **2009**, *102*, 167203.
54. Wernsdorfer, W.; Aliaga-Alcalde, N.; Hendrickson, D. N.; Christou, G. Exchange-Biased Quantum Tunnelling in a Supramolecular Dimer of Single-Molecule Magnets. *Nature* **2002**, *416*, 406–409.
55. Kahle, S.; Deng, Z.; Malinowski, N.; Tonnoir, C.; Forment-Aliaga, A.; Thontasen, N.; Rinke, G.; Le, D.; Turkowski, V.; Rahman, T. S.; *et al.* The Quantum Magnetism of Individual Manganese-12-Acetate Molecular Magnets Anchored at Surfaces. *Nano Lett.* **2012**, *12*, 518–521.
56. Miyamachi, T.; Schuh, T.; Märkl, T.; Bresch, C.; Balashov, T.; Stöhr, A.; Karlewski, C.; André, S.; Marthaler, M.; Hoffmann, M.; *et al.* Stabilizing the Magnetic Moment of Single Holmium Atoms by Symmetry. *Nature* **2013**, *503*, 242–246.
57. Kanesato, M.; Yokoyama, T. Synthesis and Structural Characterization of Ln(III) Complexes (Ln = Eu, Gd, Tb, Er, Tm, Lu) of Tripodal Tris[2-(salicylideneamino)ethyl]-amine. *Chem. Lett.* **1999**, *28*, 137.
58. Piamonteze, C.; Flechsig, U.; Rusponi, S.; Dreiser, J.; Heidler, J.; Schmidt, M.; Wetter, R.; Calvi, M.; Schmidt, T.; Pruchova, H.; *et al.* X-Treme Beamline at SLS: X-ray Magnetic Circular and Linear Dichroism at High Field and Low Temperature. *J. Synchrotron Radiat.* **2012**, *19*, 661–674.
59. Krempasky, J.; Flechsig, U.; Korhonen, T.; Zimoch, D.; Quitmann, C.; Nolting, F. Synchronized Monochromator and Insertion Device Energy Scans at SLS. *AIP Conf. Proc.* **2010**, *1234*, 705–708.
60. Lebedev, V. I.; Laikov, D. N. Quadrature Formula for the Sphere of 131-th Algebraic Order of Accuracy. *Doklady Math.* **1999**, *366*, 741–745.
61. Stoll, S.; Schweiger, A. EasySpin, A Comprehensive Software Package for Spectral Simulation and Analysis in EPR. *J. Magn. Reson.* **2006**, *178*, 42–55.
62. Khein, A.; Singh, D.; Umrigar, C. All-Electron Study of Gradient Corrections to the Local-Density Functional in Metallic Systems. *Phys. Rev. B: Condens. Matter Mater. Phys.* **1995**, *51*, 4105–4109.
63. Grönbeck, H.; Curioni, A.; Andreoni, W. Thiols and Disulfides on the Au(111) Surface: The Headgroup−Gold Interaction. *J. Am. Chem. Soc.* **2000**, *122*, 3839–3842.
64. Miller, S. D.; Kitchin, J. R. Relating the Coverage Dependence of Oxygen Adsorption on Au and Pt fcc(111) Surfaces through Adsorbate-Induced Surface Electronic Structure Effects. *Surf. Sci.* **2009**, *603*, 794–801.
65. Ali, M. E.; Sanyal, B.; Oppeneer, P. M. Tuning the Magnetic Interaction between Manganese Porphyrins and Ferromagnetic Co Substrate through Dedicated Control of the Adsorption. *J. Phys. Chem. C* **2009**, *113*, 14381–14383.
66. Larson, P.; Lambrecht, W. R. L.; Chantis, A.; van Schilfgaarde, M. Electronic Structure of Rare-Earth Nitrides Using the LSDA+U Approach: Importance of Allowing 4f Orbitals to Break the Cubic Crystal Symmetry. *Phys. Rev. B: Condens. Matter Mater. Phys.* **2007**, *75*, 045114.
67. Kresse, G.; Hafner, J. *Ab Initio* Molecular Dynamics for Liquid Metals. *Phys. Rev. B: Condens. Matter Mater. Phys.* **1993**, *47*, 558–561.
68. Kresse, G.; Furthmüller, J. Efficiency of *Ab-Initio* Total Energy Calculations for Metals and Semiconductors Using a Plane-Wave Basis Set. *Comput. Mater. Sci.* **1996**, *6*, 15–50.
69. Blöchl, P. E. Projector Augmented-Wave Method. *Phys. Rev. B: Condens. Matter Mater. Phys.* **1994**, *50*, 17953–17979.
70. Perdew, J.; Burke, K.; Ernzerhof, M. Generalized Gradient Approximation Made Simple. *Phys. Rev. Lett.* **1996**, *77*, 3865–3868.